scientific reports

Check for updates

OPEN

# Ultrasensitive electrochemical biosensor based on MXene quantum dots for prostate cancer biomarker detection

Mohammad Safarpoor[1], Arash Asfaram[2], Mehrorang Ghaedi[3]✉ & Rassoul Dinarvand[1]✉

**Prostate cancer (PSA) is among the leading causes of men's deaths worldwide and needs extremely sensitive and cost-effective diagnostic tools. In this study, an electrochemical immunosensor enhanced by polyaniline-loaded MXene quantum dots and gold nanoparticles (PANI@$Ti_3C_2$ MXene Quantum dots-Au NPs) was constructed for highly sensitive prostate-specific antigen (PSA) detection at femtogram levels. The sensor employs $V_2C$ MXene quantum dots gold-nanoparticle-decorated as signal tags to remarkably enhance electron transfer efficiency and detection sensitivity. A sandwich immunoassay strategy using MXene quantum dots gave superior selectivity and quantitation accuracy of PSA. The optimized immunosensor exhibited a large linear detection range of 2 fg $mL^{-1}$ -2 pg $mL^{-1}$ with a fantastic detection limit of 0.61 fg $mL^{-1}$. Electrochemical characterization was performed using cyclic voltammetry (CV) and electrochemical impedance spectroscopy (EIS) to confirm successful sensor fabrication and electron transfer dynamics, while differential pulse voltammetry (DPV) was employed for quantitative detection of PSA. Human serum sample validation demonstrated the clinical applicability of the platform with the presence of high specificity, reproducibility, and analytical stability. The findings place MXene quantum dots as serious contenders for next-generation biosensing technologies with a robust, scalable approach to early diagnosis of prostate cancer.**

**Keywords** Electrochemical immunosensor, Prostate-specific antigen, MXene quantum dots, Biosensing, Ultra-sensitive detection

Prostate cancer is the second most common cancer among men, accounting for approximately 7% of cancer-related fatalities worldwide. Nearly 50% of men over the age of 70 will eventually develop PSA[1]. Prostate-specific antigen (PSA) is widely recognized as a biomarker for the clinical assessment of prostate cancer[2]. Thus, the ability to detect PSA in a straightforward, rapid, and precise manner is crucial for the early diagnosis of prostate cancer and for preventing disease recurrence. Normal PSA levels in the bloodstream are typically < 4.0 ng $mL^{-1}$, while levels between 4.0 and 10.0 ng $mL^{-1}$ are considered a diagnostic "gray zone"[3]. Thus, accurate and rapid detection of PSA is essential for timely diagnosis and disease management.

Most PSA tests are conducted in advanced laboratories using conventional methods, leading to higher administrative and healthcare costs. Various analytical techniques such as colorimetric assays [4], radioimmunoassay[5], surface plasmon resonance[6], fluorescence immunoassay[7], surface enhanced Raman spectroscopy[8], chemoluminescence immunoassays[9], and electro-phoretic immunoassay[10] have been employed for PSA detection. Electrochemical immunoassays have garnered significant attention due to their high sensitivity, cost-effectiveness, and ability to detect biomarkers with precision. The sensitivity of such assays can be further enhanced through antibody quantification and the incorporation of nanoparticles to amplify signals. Incorporating engineered nanomaterials-particularly those with high conductivity and large surface area-has become a fundamental strategy for enhancing signal transduction and biorecognition. Diverse nanomaterials such as metal-organic frameworks (MOFs)[11], Graphene oxide/Cu–MOF[12], MWCNTs-COOH/Fc-COOH@COAl-LDH nanocomposite[13], carbon quantum dots[14], silica nanoparticles[15], MXenes carbon nanotube (CNT)@AuNPs[16], $Fe_3O_4$ ionic liquid[17], Polyaniline-Loaded MXene and Gold-Decorated β-Cyclodextrin[18] have been extensively employed in biosensor fabrication to immobilize antibodies.

[1]Nanotechnology Research Center, Faculty of Pharmacy, Tehran University of Medical Sciences, Tehran, Iran. [2]Medicinal Plants Research Center, Yasuj University of Medical Sciences, Yasuj, Iran. [3]Chemistry Department, Yasouj University, Yasouj 75918-74831, Iran. ✉email: m_ghaedi@mail.yu.ac.ir; dinarvand@tums.ac.ir

MXenes are a class of two-dimensional transition metal carbides, nitrides, or carbonitrides with a unique combination of properties, making them versatile materials. They are derived from layered ternary carbide, nitride, or carbonitride precursors, known as MAX phases, by selectively etching the "A" element (often aluminum) to produce a 2D layered structure. MXenes feature surfaces rich in functional groups like hydroxyl and fluorine terminations, facilitating easy surface modifications and compatibility with other materials. Certain MXenes, such as titanium carbide ($Ti_3C_2Tx$), exhibit exceptional photothermal properties, making them valuable in applications like nanocomposites for cancer treatment[19].

When MXenes are reduced to nanoscale dimensions (e.g., below 10 nm), they transform into MXene quantum dots, which retain many of the parent material's unique benefits while gaining enhanced properties such as increased specific surface area[20], improved biocompatibility[21], and easier doping or functionalization[22]. MXene quantum dots also exhibit significantly lower cytotoxicity compared to their larger MXene counterparts, making them more suitable for detecting chemical substances in biological systems[23]. These advantages position MXene quantum dots as promising materials for sensing applications, enabling the development of high-performance sensors[24].

However, the use of MXene quantum dots for biomarker detection via electrochemical techniques is still in its early stages[25]. The incorporation of PANI as a conductive polymer matrix improves dispersion and provides additional electroactive sites, while Au-NPs contribute to antibody conjugation efficiency and signal amplification[26]. Electrode fabrication via hydrothermal synthesis, drop-casting, and nanocomposite layering allows controlled optimization of morphological features, active surface area, and electrochemical accessibility. These factors jointly influence key biosensor metrics such as reproducibility, limit of detection, and dynamic response range[27,28]. The function of electrochemical biosensors is dominated by the incorporation of materials that are advanced both structurally and functionally at the electrode interface. Specifically, the synergistic utilization and the rational combination of MXene quantum dots, conductive polymers, and noble metal nanoparticles determine the sensor's operational sensitivity, electron transfer efficiency, and biofunctionality. The presented work takes advantage of the composite of PANI@$Ti_3C_2$ MXene quantum dots with AuNPs as the signal capture element, merged with $V_2C$ MXene quantum dots as signal tags, to accomplish a sandwich-type immunosensor for ultra-trace PSA detection.

## Experimental section

### Materials and reagents

Mouse anti-human monoclonal antibody ($Ab_1$), Prostate specific antigen (PSA), Mouse anti-human monoclonal antibody ($Ab_2$), Alpha-Fetoprotein (AFP), Human Immunoglobulin G (IgG), carcinoembryonic antigen (CEA), Streptavidin (STR), Glutaraldehyde (GA), Bovine serum albumin (BSA), Phosphate buffer (0.1 mol $L^{-1}$, pH 7.0), Human blood serum (healthy man), Ultrapure water, Hydrogen peroxide ($H_2O_2$), Tetrapotassium hexacyanoferrate trihydrate ($K_4[Fe(CN)_6]$)$^{3-}$, Sodium dihydrogen phosphate dehydrate ($NaH_2PO_4.2H_2O$), Disodium hydrogen phosphate dehydrate ($Na_2HPO_4.2H_2O$), Titanium aluminium carbide ($Ti_3AlC_2$) powder, Vanadium aluminium carbide ($V_2AlC$) powder, Hydrofluoric acid (HF), Hydrogen tetrachloroaurate (III) hydrate ($HAuCl_4{\cdot}3H_2O$), dimethyl sulfoxide (DMSO) and Polyaniline (PANI) powder.

### Apparatus

All electrochemical experiments, including cyclic voltammetry (CV), differential pulse voltammetry (DPV), and electrochemical impedance spectroscopy (EIS), were conducted using a Metrohm Autolab system (Autolab PGSTAT 302-N, Netherlands) controlled by Nova software (version 2.1.8). A glassy carbon electrode (GCE) was employed as the working electrode, with a Ag/AgCl electrode saturated with potassium chloride serving as the reference electrode, and a platinum wire electrode as the counter electrode.

The morphological and compositional analyses were performed using a field-emission scanning electron microscope (FE-SEM, MIRA3, Czech Republic) and an energy-dispersive X-ray analyzer (EDX, OXFORD, England). Transmission electron microscopy (TEM) was carried out using a Zeiss EM10 microscope (Germany). Additional characterization techniques included Fourier transform infrared spectroscopy (FT-IR, PerkinElmer Spectrum 2, USA), and X-ray diffraction spectroscopy (XRD, Rigaku Ultima IV, Japan).

### Approval of ethics and consent for participation

This study was conducted in full compliance with all applicable regulations and received approval from the local ethics committee of Tehran University of Medical Sciences *(Approval No.* IR.TUMS.TIPS.REC.1402.134*)*. All participants were informed about the study and provided written informed consent, which was successfully obtained prior to their participation.

### Synthesis of the titanium MXene quantum dots

A total of 2.0 g of $Ti_3AlC_2$ MAX powder was dispersed in 240 mL of hydrofluoric acid (HF, 40 wt%) and stirred for 64 h. The resulting mixture was washed with deionized (DI) water until it reached a neutral pH. The mixture was then centrifuged and repeatedly washed until the pH stabilized at approximately 6.0, after which it was dried at 60 °C. Subsequently, 0.5 g of $Ti_3C_2$ MXene was added to 10 mL of DMSO and allowed to stir for 24 h. The dispersion was then centrifuged at 3600 rpm for 10 min. The resulting solution was added to 150 mL of DI water while bubbling with argon gas, followed by sonication for 3 h. This was then centrifuged again at 3500 rpm for 1 h [29]. Subsequently, 20 mg of $Ti_3C_2$ MXene powder was completely re-dispersed in 20 mL DI water and ultrasonicated for another 30 min. The pH of the solution was adjusted at 9.0 with ammonia, and then the mixture was put into a 100 mL Teflon-sealed autoclave. The autoclave was heated at 100 °C for 6 h[30]. Scheme S1 illustrates the process of preparation.

## Synthesis of PANI@$Ti_3C_2$ MXene quantum dots and PANI@$Ti_3C_2$ MXene quantum dots -Au NPs

PANI@$Ti_3C_2$ MXene Quantum dots were synthesized by ultrasonically mixing 1.0 mg $mL^{-1}$ $Ti_3C_2$ MXene Quantum dots with 2.0 mg PANI. The resulting mixture was stirred at ambient temperature for 12 h. To prepare PANI@$Ti_3C_2$ MXene Quantum dots-Au, 500 µL of 1.0 mg $mL^{-1}$ PANI@$Ti_3C_2$ MXene Quantum Dots was added to 5 mL of freshly prepared gold nanoparticle (Au-NPs ) dispersion and mixed thoroughly. The final PANI@$Ti_3C_2$ MXene Quantum dots-Au nanocomposite was obtained by freeze-drying the mixture[26]. Gold nanoparticles (Au-NPs) were synthesized via a one-step aqueous-phase reduction method using soluble starch as both the reducing and stabilizing agent, following a previously reported procedure. In a typical synthesis, 200 µL of an aqueous solution of hydrogen tetrachloroaurate (III) trihydrate ($HAuCl_4 \cdot 3H_2O$, 0.05 mol $L^{-1}$) was added to 50 mL of an aqueous solution containing 0.2 wt% soluble starch under vigorous magnetic stirring. The pH of the mixture was adjusted to pH 11.0 ± 0.2 using 0.05 mol $L^{-1}$ sodium hydroxide (NaOH) solution. The reaction mixture was stirred at ambient temperature for 1 h, during which a light pink hue appeared, indicating the nucleation of Au-NPs. The solution was then maintained at 70 °C for 6 h. The progression to a deep burgundy color confirmed the completion of the reduction process and the successful formation of stable colloidal gold nanoparticles[31].

## Preparation of GCE modification with PANI@$Ti_3C_2$ MXene quantum dots-Au composite

The sensor fabrication used a glassy carbon electrode (GCE) with a 3 mm diameter as its working electrode. The GCE surface received mechanical polishing with 0.05 µm $Al_2O_3$ slurry before undergoing five-minute ultrasonic cleaning sessions with ethanol and ultrapure water to remove surface contaminants. The PANI@$Ti_3C_2$ MXene Quantum Dots-Au nanocomposite required ultrapure water to create a 1.0 mg $mL^{-1}$ (w/v%) stock suspension. The dispersion process involved ultrasonic treatment for thirty minutes at room temperature to achieve uniform distribution while stopping nanoparticle aggregation. The electrochemical system required ultrapure water as the dispersing solvent because it provides system compatibility and contains no interfering ions. The 1.0 mg $mL^{-1}$ nanocomposite suspension received a 3.0 µL drop onto the cleaned GCE surface which dried naturally at room temperature for 20 min under dust-free conditions.

## Immunosensor fabrication

The prostate-specific antigen (PSA) antibody ($Ab_1$) was covalently attached to the PANI@$Ti_3C_2$ MXene Quantum dots-Au/GCE via the interaction between the gold atoms in the composite and the amino ($-NH_2$) groups of the antibody. After preparing the PANI@$Ti_3C_2$ MXene Quantum Dots-Au/GCE, the electrode was immersed in an Ab1 solution (80 µg $mL^{-1}$ in 0.01 mol $L^{-1}$ PBS, pH 7.0) and incubated for 40 min at 37 °C. Following incubation, unbound $Ab_1$ was thoroughly rinsed off using PBS. To block nonspecific binding sites, the electrode was further incubated with 1% (w/w) bovine serum albumin (BSA) at 37 °C for 40 min. After rinsing with PBS to remove residual BSA, the resulting immunosensor was finalized and designated as BSA/$Ab_1$/PANI@$Ti_3C_2$ MXene Quantum dots-Au/GCE. Subsequently, varying concentrations of PSA were applied to the BSA/$Ab_1$/PANI@$Ti_3C_2$ MXene Quantum dots-Au/GCE and incubated for 40 min at 37 °C. To eliminate unbound PSA proteins, the immunosensor (PSA/BSA/Ab1/PANI@$Ti_3C_2$ MXene Quantum dots-Au/GCE) was washed with 0.1 mol $L^{-1}$ PBS (pH 7.0).

## Preparation of $Ab_2$ bioconjugates based on $V_2C$ quantum dots@Au-NPs

$V_2C$ MXene was synthesized by etching the $V_2AlC$ phase. In a standard procedure, 1 g of $V_2AlC$ powder was gradually submerged in 10 mL of HF (50 wt%) solution in a Teflon bottle and stirred vigorously at room temperature for 72 h to remove the Al layer. The resultant mixture was washed with deionized water and centrifuged at 6000 rpm for 5 min. The process was repeated several times until the supernatant reached a pH of approximately 7.0. Vacuum filtration and vacuum drying at 60 °C for 8 h were employed to yield the Layered $V_2C$ MXene product[32]. Next, 0.5 g of $V_2C$ MXene was added to 10 mL of DMSO and stirred for 24 h. Suspension was centrifuged at 3600 rpm for 10 min, and dispersion was added into 150 mL of deionized water. Argon gas was bubbled into suspension and then sonicated for 3 h. Further centrifugation at 3500 rpm for 1 h yielded the final product[29]. The $V_2C$ MXene Quantum dots were subsequently synthesized using the pre-prepared $V_2C$ MXene as precursors in a hydrothermal treatment at 100 °C in aqueous ammonia solution[30].

The $V_2C$ MXene Quantum Dots@Au-NPs composite was synthesized based on previously reported procedures with minor modifications. Briefly, 6 mg of $V_2C$ MXene Quantum dots was ultrasonically dissolved in 3 mL of ultrapure water for 30 min to give a uniform solution. Next, 500 µL of $HAuCl_4 \cdot 3H_2O$ aqueous solution (30 µM) was gradually added while gently stirring. After a 10-minute reaction, the resulting $V_2C$ MXene Quantum dots@Au-NPs suspension was centrifuged at 8000 rpm for 5 min, and the precipitate was collected[33]. A total of 50 mg of $V_2C$ MXene Quantum dots@Au-NPs was resuspended in 50 mL of ultrapure water. After 60 min, the suspension underwent several centrifugation cycles with ultrapure water. For the conjugation, 20.0 µL of $Ab_2$ (30.0 µg $mL^{-1}$) was attached to the composite through the interaction between gold atoms and the $-NH_2$ groups of $Ab_2$. The resulting mixture was dispersed in 0.1 mol $L^{-1}$ PBS (pH 7.0) and stored at 4 °C (Scheme S2). A sandwich-type immunoassay was developed for the sensitive electrochemical detection of PSA Following the preparation of the PSA /BSA/$Ab_1$/PANI@$Ti_3C_2$ MXene Quantum dots-Au/GCE, 15.0 µL of the $Ab_2$ bioconjugate solution was applied to the electrode surface for 50 min to facilitate the immune reaction. The immunosensor ($V_2C$ MXene Quantum dots@Au/$Ab_2$/PSA /BSA/$Ab_1$/PANI@$Ti_3C_2$ MXene Quantum dots-Au/GCE) was washed with PBS (0.1 mol $L^{-1}$, pH 7.0) to remove unbound $Ab_2$ bioconjugates.

Finally, for the quantitative electrochemical detection of PSA, 20 µL of 30.0 mM $H_2O_2$ was added and allowed to react for 20 min. The treated electrodes were then analyzed using DPV measurements conducted in the potential range of -0.5 to 0.5 V.

## Results and discussion

### Identification of MXene quantum dots

FT-IR analysis of the Titanium MXene Quantum dots is shown in (Fig. 1). As indicated in the figure, the peaks at 3494 and 3002 $cm^{-1}$ originated from the stretching modes of Hydroxyl and amine functional groups (O-H and N-H), respectively[34]. The peaks at 578, 114, and 1731 $cm^{-1}$ correspond to the stretching vibrations of Ti-O, C-F, and C = O bonds, while the peak at 1319 $cm^{-1}$ corresponds to the bending vibrations of O–H[35–38].

The morphology and microstructure of the $Ti_3AlC_2$ MAX phase, $Ti_3C_2$ MXene, $Ti_3C_2$ MXene (treated with DMSO), and $Ti_3C_2$ MXene Quantum dots were examined using Field Emission Scanning Electron Microscopy (FE-SEM). The $Ti_3AlC_2$ MAX phase exhibits a dense structure.

The multilayer configuration confirms the morphology of $Ti_3C_2$ MXenes, which were transformed into single or multilayer MXenes via ultrasonication in the presence of DMSO solvent, as well as into MXene quantum dots (Fig. 2a-d).

To further investigate $Ti_3C_2$ MXene Quantum dots, Energy-dispersive X-ray spectroscopy (EDX) analysis was used to identify their elemental compositions. EDX analysis validated the presence of carbon (C) and titanium (Ti) elements, which are characteristic of MXene Quantum dots[39]. The EDX findings also confirmed the successful removal of the Al element, with only Ti and C elements remaining in the MXene Quantum dots nanostructure (Fig. 2e, f).

Additionally, the PANI@$Ti_3C_2$ MXene QDs-Au and PANI@$Ti_3C_2$ MXene Quantum dots (Fig. 3a, b), as well as the $V_2AlC$ MAX phase, $V_2C$ MXene, $V_2C$ MXene (treated with DMSO), and $V_2C$ MXene Quantum dots composites were examined using FE-SEM. The MAX phase exhibited a dense structure, while the MXene phases displayed a layered structure (Fig. 4a-c).

Figure 5a, b shows the layered structure of MXene quantum dots, as well as the presence and uniform distribution of gold nanoparticles. To further investigate $V_2C$ MXene quantum dots, EDX analysis was used to identify its elemental compositions. The presence of carbon (C) and vanadium (V) elements was confirmed (Fig. 5c).

TEM images of MXene quantum dots in (Fig. 6a, b) show that they are uniformly dispersed without significant aggregation. The average size of the $Ti_3C_2$ MXene Quantum dots was estimated to be $3.29 \pm 0.06$ nm, while the size of the $V_2C$ MXene quantum dots is about 2.92 nm, as shown in the histogram of the MXenes, confirming that the MXenes are indeed quantum dots (Fig. 6c, d). X-ray diffraction (XRD) analysis was used to determine the nature of $Ti_3C_2$ MXene Quantum dots by providing information about their crystallographic structure, lattice parameters, and phase composition.

The XRD analysis also illuminated the atomic arrangement of the $Ti_3C_2$ MXene Quantum dots. (Fig. 7) illustrates that the $Ti_3C_2$ MXene Quantum dots exhibit a layered structure, which is similar to that of other layered MXenes. Following the etching of the MAX phase, the prominent (1 0 4) peak of $Ti_3AlC_2$ at 39.0° disappears in the $Ti_3C_2$ MXene[40]. Additionally, the broadening of diffraction peaks in $Ti_3C_2$ MXene Quantum dots compared to their bulk counterparts indicates a reduction in crystallite size, a hallmark of quantum confinement effects[41]. The XRD patterns of $Ti_3C_2$ MXene Quantum dots reveal an increase in interlayer distance owing to the removal of intercalated species and the incorporation of functional groups such as hydroxyl (-OH) and fluoride ($F^-$). The shift of the (0 0 4) peak towards higher angular values signifies accordion-like structural changes brought about by hydrothermal treatment. These changes enhance the electrochemical properties of $Ti_3C_2$ MXene Quantum dots, which make them extremely suitable for biosensing purposes[42].

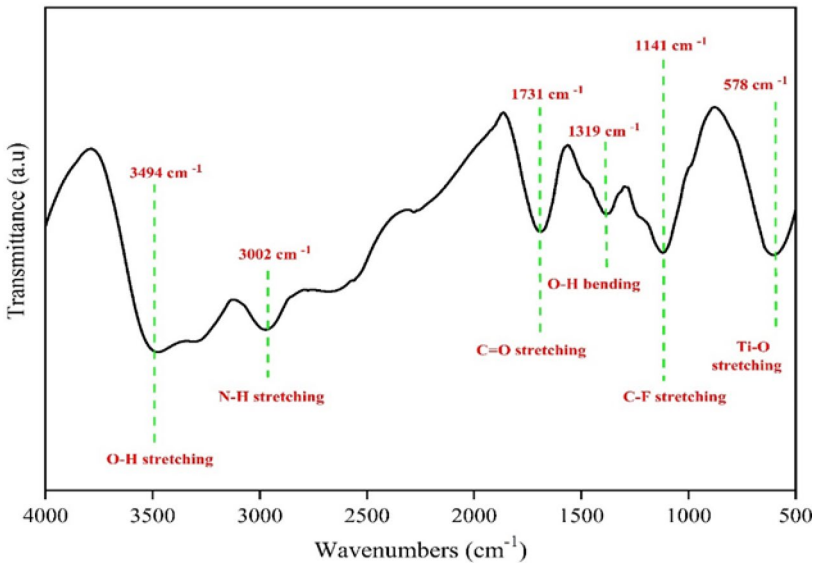


**Fig. 1**. FTIR spectra of the MXene QDs sheets.

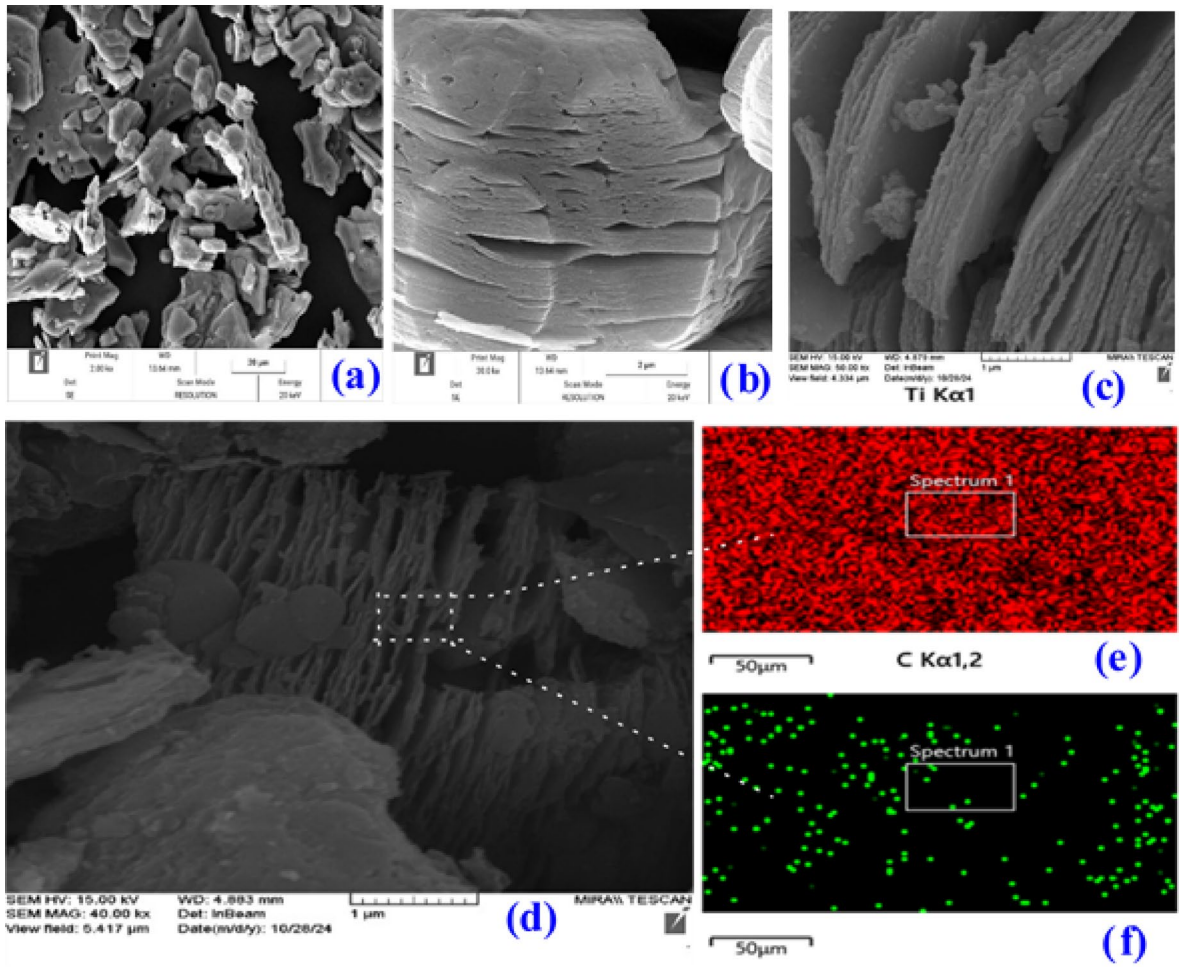


**Fig. 2**. FE-SEM images (**a**,**b**,**c**,**d**) of the original bulk material $Ti_3AlC_2$, the as-obtained layered $Ti_3C_2$ MXene, $Ti_3C_2$ MXene (DMSO), and $Ti_3C_2$ MXene QDs; FE-SEM-EDX elemental mapping images (**e**, **f**) of the pristine $Ti_3C_2$ MXene QDs sheets.

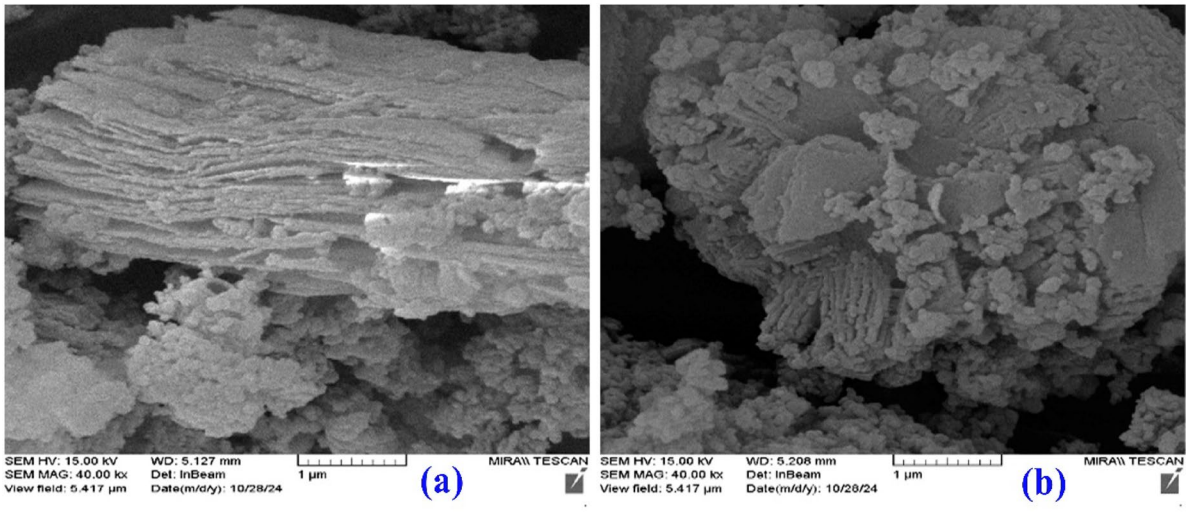


**Fig. 3**. FE-SEM images of (**a**) the PANI@$Ti_3C_2$ MXene Quantum dots-Au and (**b**) the PANI@$Ti_3C_2$ MXene Quantum dots.

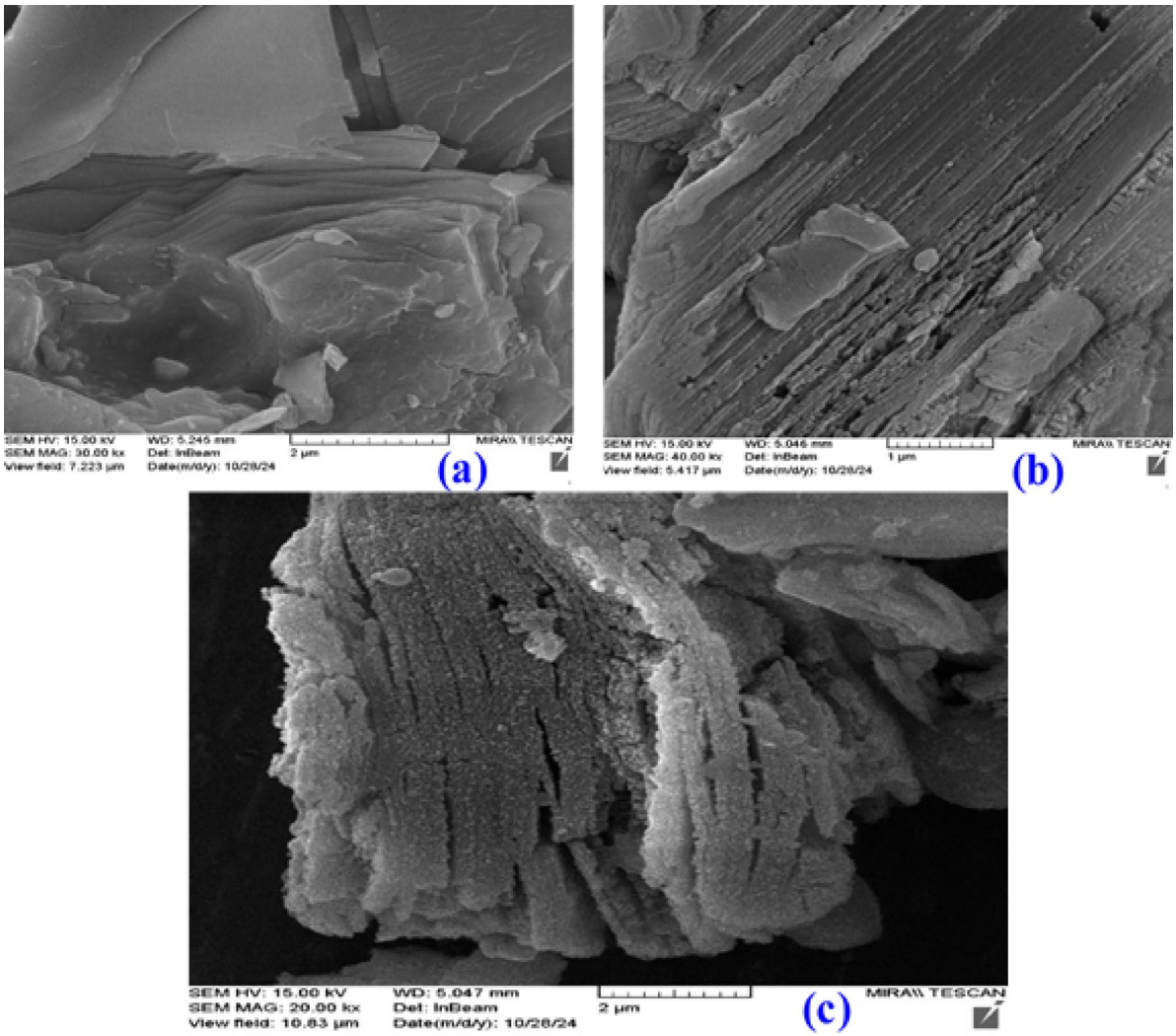


**Fig. 4**. FE-SEM images of (**a**) the $V_2AlC$ MAX phase, (**b**) the $V_2C$ MXene, and (**c**) the $V_2C$ MXene (DMSO).

## Electrochemical behavior of the immunosensor

In (Fig. 8a, b) depict the CV and electrochemical impedance spectroscopy (EIS) curves obtained during the stepwise fabrication of the immunosensor in a 5 mM $[Fe(CN)_6]^{3-/4-}$ solution with 0.1 mol $L^{-1}$ KCl. These electrochemical techniques provide key insights into the electrode modification process, confirming successful sensor construction and assessing electron transfer dynamics.

To improve the biosensor's electrochemical performance, polyaniline (PANI) was combined with MXene quantum dots to create a conductive and functional composite interface. The main interaction mechanisms include hydrogen bonding between the $-NH_2$ and -NH groups of PANI and the surface terminations (-OH, $O^{2-}$, $F^-$) of MXenes. There is also π-π stacking between the conjugated PANI backbone and the structure less MXene basal planes, along with electrostatic stabilization from the positively charged PANI matrix interacting with the negatively charged MXene surfaces. These combined forces lead to better dispersion, increased electron transfer, and higher redox activity of the nanocomposite. The PANI@MXene configuration increases the interface area of this biosensor. CV analysis is a critical method for the description of redox activity of modified electrodes. Bare GCE has very low peak currents, indicating limited electron transfer kinetics. Peak currents are dramatically increased following modification with the PANI@$Ti_3C_2$ MXene quantum dots-Au nanocomposite, indicating the enhanced efficiency of electron transfer through the conductivity of MXene quantum dots and gold nanoparticles (Fig. 8a). $Ab_1$ (primary antibody) binding resulted in a reduction of the current response. This is because of the insulating nature of biomolecules, which prevents the flow of electrons on the electrode surface. Further reductions in current intensity are observed with bovine serum albumin (BSA) immobilization and PSA antigen, again demonstrating these biomolecules to be charge-blocking agents[43].

Research shows that polyaniline (PANI) plays an important role in the conductivity of the electrode and also provides active sites for the electrochemical process via its redox-active backbone. $Ti_3C_2TX$, on the other hand, has high metallic conductivity, high surface area and a large number of surface terminations (–OH, $O^{2-}$, $F^-$) which can easily make the electrons move quickly and also immobilize the biomolecules. The MXenes, as opposed

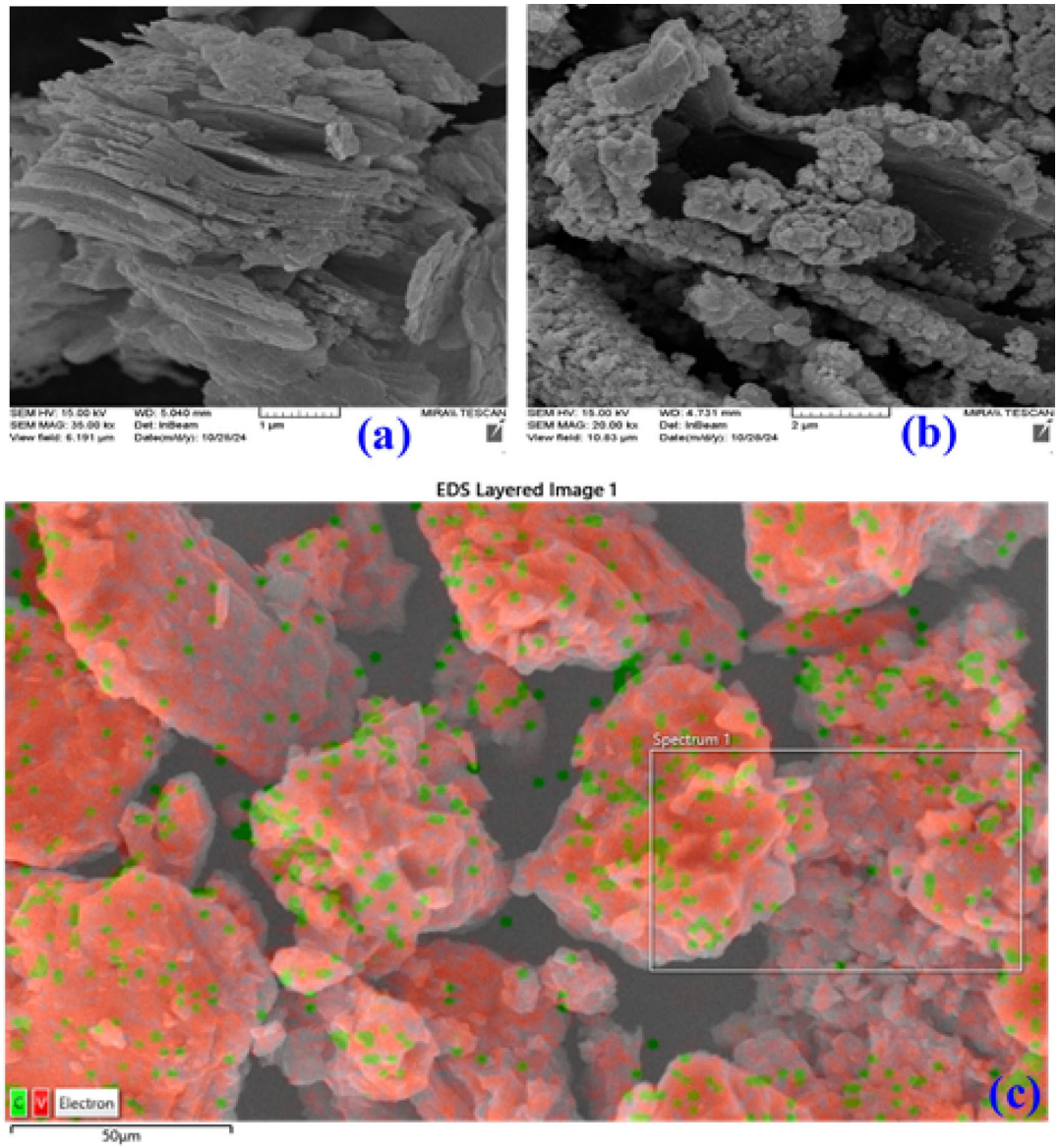


**Fig. 5**. FE-SEM images (**a**,**b**) of the $V_2C$ MXene Quantum dots and $V_2C$ MXene Quantum dots-Au NPs; FE-SEM-EDX elemental mapping images (**c**) of the pristine $V_2C$ MXene QDs sheets.

to PANI, have a different structure of layers which allow for ion intercalation and fast charge transport, thus, reducing the interfacial resistance. Moreover, PANI can help with the film-forming ability and the mechanical flexibility of the electrode, while MXenes are responsible for the charge transfer kinetics, the electrochemical stability and the catalytic activity which makes them the main source of biosensor sensitivity improvement[44–46]. EIS is a highly sensitive method for evaluating the interfacial charge transfer resistance (Rct) of electrochemical systems. In the Nyquist plots presented in (Fig. 8b), the semicircular diameter corresponds to the Rct value, reflecting changes in surface conductivity during immunosensor construction Initially, the bare GCE, which has a large Rct, corresponds to a simple surface with low conductivity. Upon deposition of the PANI@$Ti_3C_2$ MXene Quantum dots-Au NPs composite, there is a significant decrease in impedance, as per the conductive nature of MXenes and gold nanoparticles, which favor electron transfer. The sequential functionalization with Ab1, BSA and PSA antigen, the Nyquist semicircle grows progressively, as a sign of an increase in Rct. This trend again verifies the insulating nature of biomolecular layers and confirms step-by-step, successful assembly of the immunosensor[47,48].

## Optimization of immunosensor conditions

Several factors, including the pH of the buffer, concentrations of $H_2O_2$ and $Ab_2$, and incubation times for $Ab_1$ and $Ab_2$, significantly influence the immunosensor's electrochemical performance. These parameters were optimized as follows:

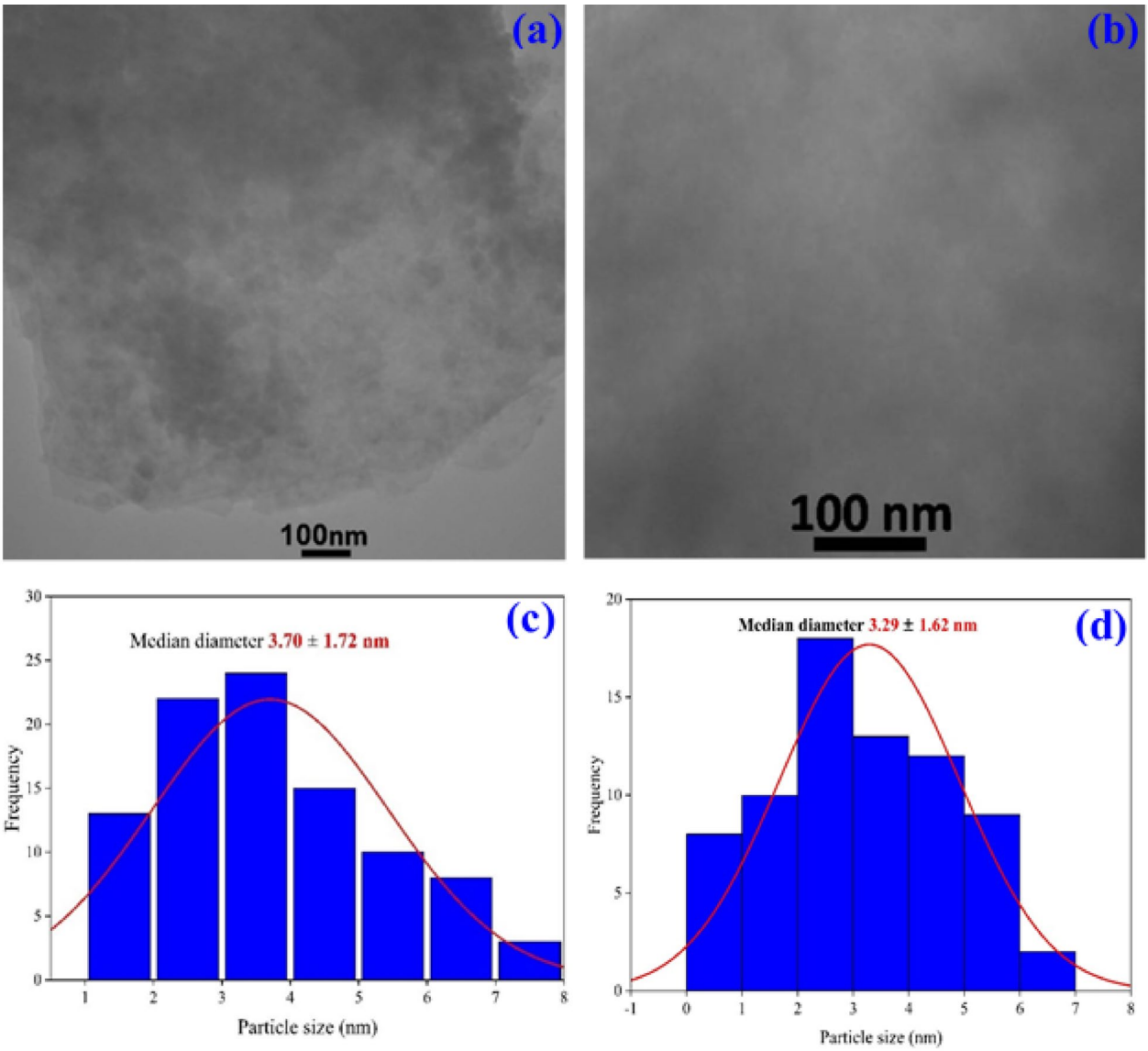


**Fig. 6**. TEM images (**a**,**b**) and histograms (**c**,**d**) of Titanium and Vanadium quantum dots of MXenes, respectively.

The pH of the phosphate buffer is highly important in the electrochemical behavior of the immunosensor as it directly impacts the activity and stability of the immobilized proteins. The establishment of the pH conditions which are the best ones for the maximum antigen-antibody interaction is crucial because that way the immunosensor becomes more sensitive and reliable. Electrochemical Response to pH alterations: The CV and DPV measurements were conducted using 0.1 mol $L^{-1}$ phosphate buffer solutions of differing pH between the range 3.0–10.0 (Fig. 8c, d). The data obtained, it has been observed the current response rises from pH 3.0–7.0, showing that there is heightened protein activity with improved electron transfer kinetics. This behavior arises from the fact that the intermediate ionized state of the antibody-antigen complex enables the most effective way toward the interface for the electrochemical charge transfer. Moreover, under very high alkaline conditions (pH > 8.0), the bio-components lost the originality of the structural form and the response of electron transfer diminished. Thus, for the best immunosensor performance, 7.0 pH was selected to be the optimum condition for the detection procedure[49,50].

The incubation time for $Ab_1$ and $Ab_2$ was examined to identify the optimal duration for the immunoreaction. For $Ab_1$, incubation times ranging from 10 to 70 min were tested (Figure S1a). The inhibition ratio of the current response increased with longer incubation times, peaking at 40 min. Beyond this point, the inhibition ratio declined, likely due to the detrimental effects of prolonged exposure or temperature on biomolecular function. Consequently, an incubation time of 40 min was deemed optimal for $Ab_1$.

Similarly, the response of the immunosensor to $Ab_2$ conjugated with $V_2C$ MXene quantum dots @Au was analyzed at varying incubation times (Figure S1b). An incubation time of 40 min was also found to be ideal for the $Ab_2$ bioconjugate interaction.

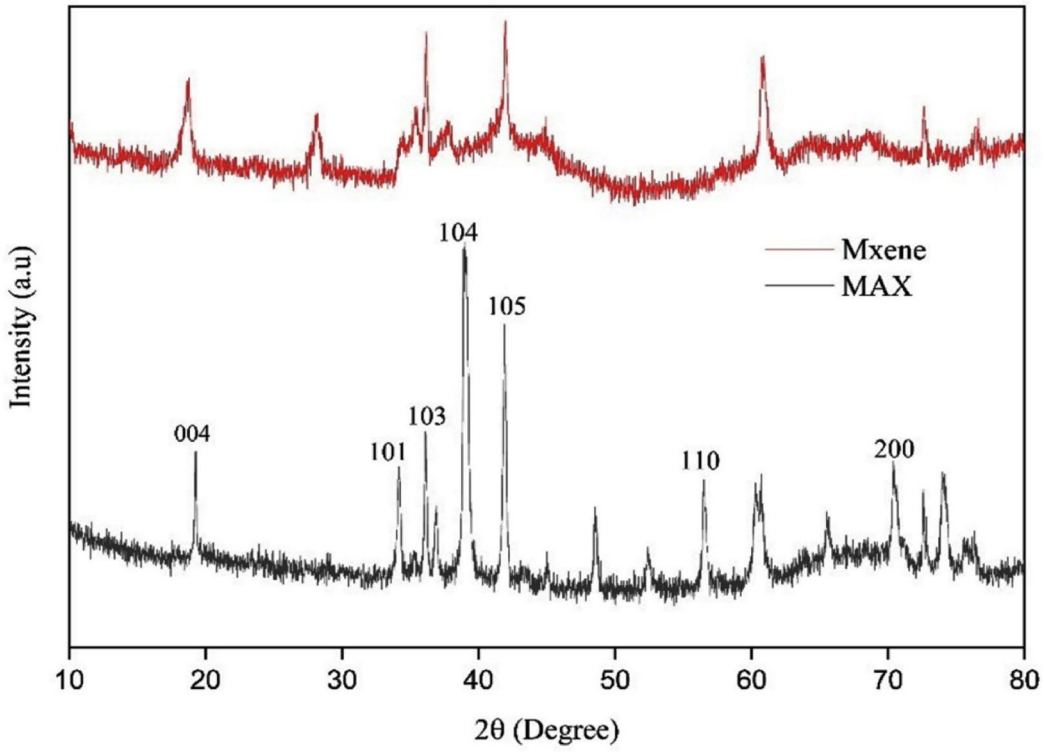


**Fig. 7**. The XRD patterns of the $Ti_3AlC_2$ MAX phase and MXene QDs.

The concentration of $Ab_2$ conjugated with $V_2C$ MXene quantum dots@Au nanoparticles was optimized to maximize signal amplification. As shown in (Figure S1c), the peak current increased with $Ab_2$ concentrations up to 30 μg $mL^{-1}$, after which it plateaued or slightly diminished. Thus, 30 μg $mL^{-1}$ was selected as the optimal $Ab_2$ concentration.

Hydrogen peroxide ($H_2O_2$) is a important compound as the redox probe in electrochemical immunosensors, which is involved in the catalytic reaction and the signal amplification. The adjustment of its concentration to time is a must for great sensitivity and the efficiency of detecting PSA. The determination of the correlation between the concentration of $H_2O_2$ and immunosensor's performance was done using the technique of DPV (Figure S1d). The current response increased with $H_2O_2$ concentration up to 30 mM, which means a better catalytic activity but most importantly it shows a faster electron transfer between the analyte and the electrode. At concentrations of 30 mM and above, the surplus of the $H_2O_2$ led to a low effect of the catalytic reaction so the current also fell down. This reduction might be understood as really high $H_2O_2$ concentrations that caused oxidative stress to the biomolecular components; that is, oxidative stress jeopardized both enzymes and the electrode surface. Consequently, 30 mM $H_2O_2$ was determined to be the optimal concentration for achieving maximum immunosensor performance[51].

## Validation

Blood specimens from healthy donors were collected from *Shahid Jalil Hospital in Yasouj*, *Iran*, and stored frozen until used. Detection of PSA by the immunosensor was done by diluting the samples at a 1:1 ratio with distilled water. To simulate conditions in cancer patient with elevated PSA levels, varying concentrations of standard PSA solutions were spiked into the serum samples. Using the standard addition method, recoveries of 100.00% to 100.50% were obtained, exhibiting very high accuracy.

The electrochemical abilities of the immunosensor constructed were evaluated by DPV in the presence of different PSA concentrations. As depicted in Fig. 9a, a clear trend was observed: the oxidation peak current decreased proportionally with increasing PSA concentration, confirming the high sensitivity of the immunosensor.

The reduction mentioned was due to the biomolecular layers being insulative in nature, which were formed during the sandwich-type immunoassay, and thus progressively blocked the electron transfer at the electrode interface. Along with the current shifts, there was a prominent anodic potential shift at the peak. The change in peak potential originates from the changed interface dynamics due to the repeated immunoreactions. By the time the PSA antigen is caught by $Ab_1$ and connected with $Ab_2$@$V_2C$ MXene QDs@Au-NPs nanoconjugate, the electrode surface that is inactive from the point of view of the electrochemical reactions gets covered with biomolecular layers more and more. The sequential layering leads to charge redistribution, increased steric hindrance, and changed electron transfer routes. All these raise the overpotential that is needed for the oxidation

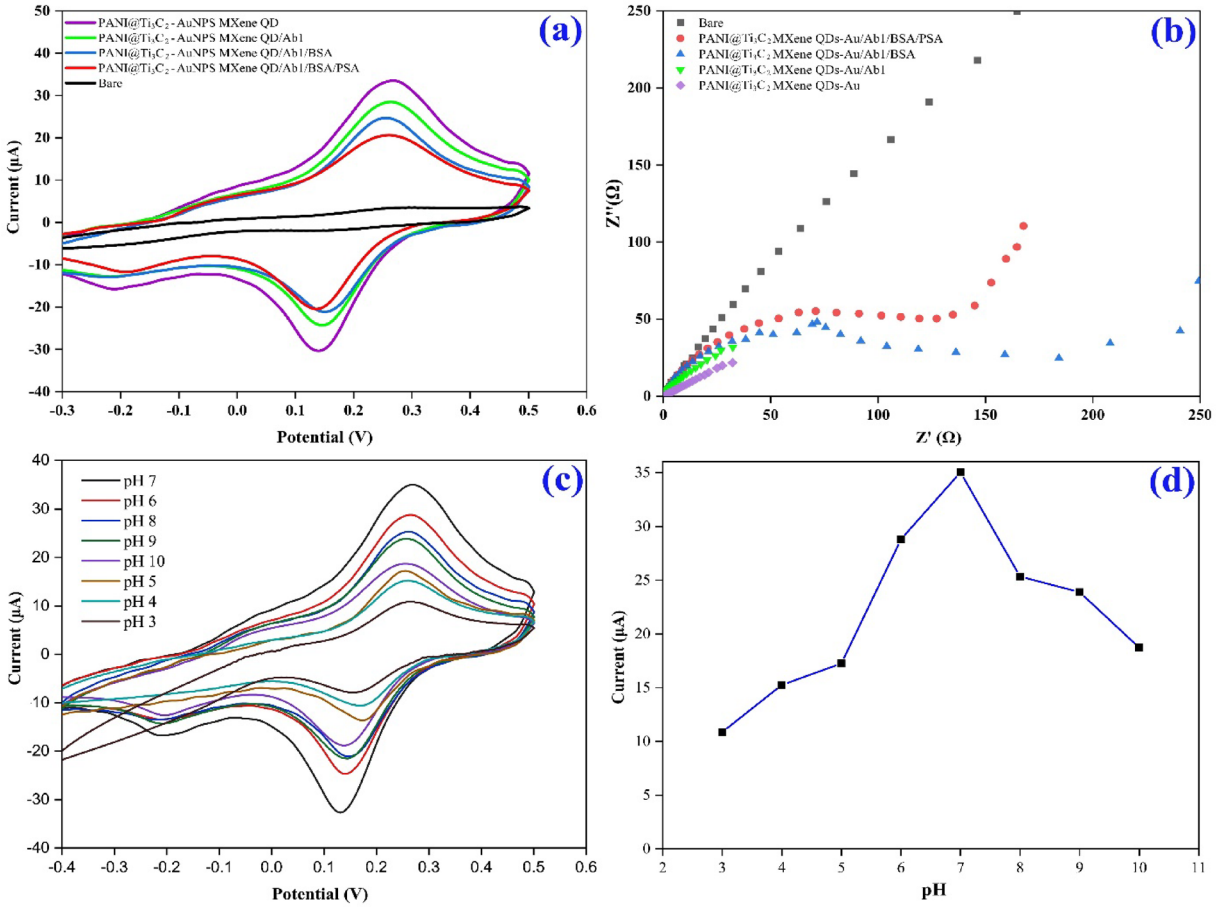


**Fig. 8**. CV (**a**) EIS (**b**) curves obtained from different electrodes in the fabrication of the immunosensor in $[Fe(CN)_6]^{3-/4-}$ solution. and Effect of pH on the immunosensor response (**c**, **d**).

of the electroactive species (i.e., $H_2O_2$), resulting in the observed Ep shift. This case shows the signal decrease not only as a result of the lower conductivity but also due to the changing electrochemical impedance at the interface. These shifts in peak potential have been observed in biosensors in which restricted electron mobility as a result of high-density surface functionalization and interfacial electrostatics alter the redox potential of the system[47,48,51]. The electrochemical sensitivity of the device are thus maintained through this alteration, also provides a further qualitative indication of successful antigen capture and immunocomplex formation. In Fig. 9b, the calibration plot with a very low detection limit of 0.61 fg $mL^{-1}$ ($S/N = 3$) is demonstrated, showing the linearity between peak current and PSA concentration in the range 2 fg $mL^{-1}$ to 2 pg $mL^{-1}$.

These metrics strongly affirm the sensor's suitability for ultra-trace biomarker detection. In future iterations, both current amplitude and peak potential shift may be co-utilized to enhance dual-signal validation protocols in biosensing applications. Comparisons with other electrochemical PSA immunoassays (Table 1) indicate that the developed sensor performs comparably or better in certain instances.

Reproducibility was assessed using intra-assay and inter-assay variations. For intra-assay precision, PSA analysis was performed on three immunosensors, with six replicates each (Table 2). The relative standard deviation (RSD) values reflect a excellent repeatability of the immunosensor.

The immunosensor's potential in the PSA detection using human serum was confirmed with the standard addition method. The samples were diluted to 50-fold and spiked with differing PSA concentrations. The results ranged from 100.125% to 100.286% at +100 mV (Table 3) confirming the method's accuracy, precision, and specificity for real-world applications.

The principle of selectivity was examined by challenging different immunosensor samples with five biomarkers mixtures, containing IgG, streptavidin (STR), carcinoembryonic antigen (CEA), alpha-fetoprotein (AFP), and a mixture of them all. The solutions were as follows 0.50 pg $mL^{-1}$ PSA, 1.50 pg $mL^{-1}$ CEA, IgG, STR, and AFP in 0.1 mol $L^{-1}$ phosphate-buffered saline (pH 7.0). The results were unambiguously in favor of the immunosensor's selectivity for PSA detection, as non-PSA biomarkers exhibited no change in the measurements (Fig. 9c).

The assessment of stability was done by keeping the immunosensors at 4 °C for a period of 30 days. Besides the current response they got by using the 0.5 pg $mL^{-1}$ PSA concentration, the responses which were obtained after the 30-day storage visualized 96.34% of its initial value, thus assuring a satisfactory stability of the immunosensor (Fig. 9d). To check repeatability, 30 consecutive voltammograms were recorded in the presence

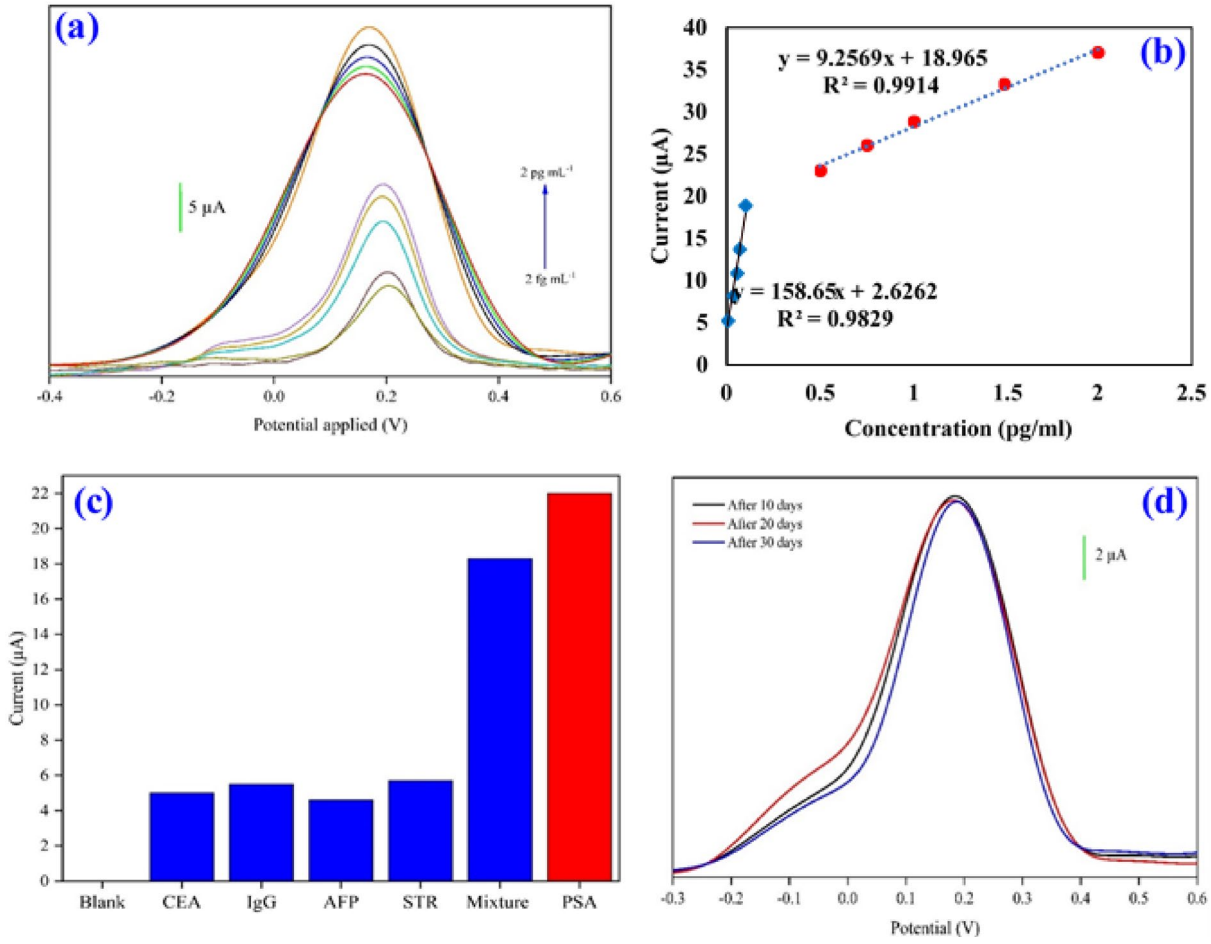


**Fig. 9**. (**a**) DPV curves of the immunosensor in the presence of different concentration (2 fg $mL^{-1}$ to 2 pg $mL^{-1}$) PSA, (**b**) the calibration curve for determination of PSA, (**c**) the currents obtained on the developed immunosensor, and (**d**) inter-day measurements for the stability of the prepared immunosensor.

| Electrodes | Linear Range | LOD | Refs. |
|---|---|---|---|
| MOF-235 | 100.0 fg $mL^{-1}$– 10.0 µg $mL^{-1}$ | 63.24 fg $mL^{-1}$ | 51 |
| NiFe PBA/AuNPs | 0.5 pg $mL^{-1}$ – 1000 pg $mL^{-1}$ | 0.23 pg $mL^{-1}$ | 52 |
| PSA /α-$F_2O_3$/$Fe_3O_4$@Au | 100 fg $mL^{-1}$- 100 ng $mL^{-1}$ | 0.78 pg $mL^{-1}$ | 53 |
| $MoS_2$/Pt@Au-nanoprism/PDA | 0.0001 ng $mL^{-1}$- 100 ng $mL^{-1}$ | 0.1 pg $mL^{-1}$ | 54 |
| $NH_2$-VMSF | 10 pg $mL^{-1}$– 1 µg $mL^{-1}$ | 8.1 pg $mL^{-1}$ | 55 |
| CS–rGO | 10 fg $mL^{-1}$- 1 ng $mL^{-1}$ | 1.9 pg $mL^{-1}$ | 56 |
| AuNWs/anti-PSA doped polypyrole | 10 fg $mL^{-1}$- 10 ng $mL^{-1}$ | 0.3 pg $mL^{-1}$ | 57 |
| GS–QD | 0.005 ng $mL^{-1}$- 10 ng $mL^{-1}$ | 3 pg $mL^{-1}$ | 58 |
| Quince seed mucilage-GNPs-SNPs | 0.1 pg $mL^{-1}$ – 100 ng $mL^{-1}$ | 0.078 pg $mL^{-1}$ | 59 |
| PANI@$Ti_3C_2$-Au-NPs MXene Q.Ds | 2 fg $mL^{-1}$- 2 pg/mL | 0.61 fg $mL^{-1}$ | This study |

**Table 1**. Evaluation of the created immunosensor for the detection of PSA with different electrodes.

of 20.0 mM $H_2O_2$. The responses at + 100 mV were highly consistent, with an RSD of 0.237, which confirmed the reliability of the immunosensor.

## Conclusions

This study presents the development of a highly sensitive electrochemical immunosensor that, employing PANI@$Ti_3C_2$ MXene quantum dots-Au-NPs, is designed for the detection of femtogram levels of prostate-specific antigen (PSA). The sensor was designed and optimized systematically. The addition of gold nanoparticles, along with the complementary integration of $Ti_3C_2$ and $V_2C$ MXene quantum dots, enabled the fabrication of a biosensor interface of high strength that had outstanding analytical capabilities. Effective $Ab_1$ binding was

| Added (pg $mL^{-1}$) | Intra-day | | Inter-day | |
|---|---|---|---|---|
| | Found [a] (pg $mL^{-1}$) | Precision [b] (%) | Found [a] (pg $mL^{-1}$) | Precision [b] (%) |
| 0.3 | 0.3001 | 0.151 | 0.3002 | 0.152 |
| 0.6 | 0.6001 | 0.139 | 0.6001 | 0.140 |
| 0.9 | 0.9001 | 0.148 | 0.9002 | 0.137 |

**Table 2**. Intra-day and inter-day precision of PSA ($n = 6$). [a] Mean. [b] Precision %: Relative Standard Deviation (RSD).

| Plasma sample [a] | Added PSA (pg $mL^{-1}$) | Found PSA (pg $mL^{-1}$) | Recovery (%) |
|---|---|---|---|
| Sample (1) | 0.500 | 0.499 | – |
| Sample (2) | Sample (1) + 0.100 | 0.601 | 100.170 |
| Sample (3) | Sample (1) + 0.200 | 0.702 | 100.286 |
| Sample (4) | Sample (1) + 0.300 | 0.801 | 100.125 |

**Table 3**. The recovery of PSA ($N = 6$). [a] Containing 0.50 pg $mL^{-1}$ PSA, 1.50 pg $mL^{-1}$ CEA, 1.50 pg $mL^{-1}$ IgG, 1.50 pg $mL^{-1}$ STR, 1.50 pg $mL^{-1}$ AFP.

made possible by the high conductivity, large number of functional groups, and decreased interfacial resistance provided by $Ti_3C_2$ QDs scattered on the electrode. By catalyzing $H_2O_2$ oxidation and increasing signal intensity, $V_2C$ QDs@Au-NPs, which were introduced via $Ab_2$ conjugation, showed remarkable redox activity. Stable antibody coupling and redox current amplification were facilitated by the Au-NPs that were woven throughout both components. The best working conditions showed that the sensor had a range from 2 fg $mL^{-1}$ to 2 pg $mL^{-1}$ which is linear and a detection limit of only 0.61 fg $mL^{-1}$, much more sensitive compared to other biosensing methods. The introduction of MXene quantum dots played a crucial role in helping the sensor to enhance the electron transfer efficiency, thus increase the signal amplification. The sensor was not only selective, but also demonstrated that no interference was observed from co-existing biomarkers with a high degree of stability, reproducibility, and analytical performance, thus confirming its clinical diagnostics applicability. Validation using human serum samples confirmed its feasibility for early prostate cancer detection. The outcomes of the research emphasized the importance of MXene quantum dots in terms of the driving force of next generation biosensing technologies, thus contributing to the cause of advanced nanomaterial-based electrochemical platforms with bio-compatibility and functional versatility.

## Data availability

The authors declare that the data supporting the findings of this study are available within the paper, a request for more detailed data should be sent to the corresponding authors with the permission of all authors.

Received: 7 July 2025; Accepted: 30 October 2025
Published online: 28 November 2025

## References

1. Sandúa, A. et al. PSA reactivity in extracellular microvesicles to commercial immunoassays. *Clin. Chim. Acta*. **543**, 117303 (2023).
2. Yao, J., Wang, Y., Dai, Y. & Liu, C. C. Bioconjugated, Single-Use biosensor for the detection of biomarkers of prostate cancer. *ACS Omega*. **3**, 6411–6418 (2018).
3. Takano, E. et al. Highly sensitive Fluoro-Immunosensing for biomarker detection using an automatic pipette Tip-Type biosensing system. *ACS Omega*. **4**, 1487–1493 (2019).
4. Liu, W., Yao, Y., Liu, Q. & Chen, X. Nanoenzyme hydrogel Film-Based portable Point-of-Care testing platform for Double-Signal visual detection of PSA. *Anal. Chem.* **96**, 9909–9916 (2024).
5. Chen, Y. T. et al. Quantitative analysis of prostate specific antigen isoforms using Immunoprecipitation and stable isotope labeling mass spectrometry. *Anal. Chem.* **87**, 545–553 (2015).
6. Besselink, G. A. J., Kooyman, R. P. H., van Os, P. J. H. J., Engbers, G. H. M. & Schasfoort, R. B. M. Signal amplification on planar and gel-type sensor surfaces in surface plasmon resonance-based detection of prostate-specific antigen. *Anal. Biochem.* **333**, 165–173 (2004).
7. Korram, J., Anbalagan, A. C., Banerjee, A. & Sawant, S. N. Bio-conjugated carbon Dots for the bimodal detection of prostate cancer biomarkers via sandwich fluorescence and electrochemical immunoassays. *J. Mater. Chem. B*. **12**, 742–751 (2024).
8. Armero, L. et al. Multiplex determination of glycan profiles on urinary Prostate-Specific antigen by Quartz-Crystal microbalance combined with Surface-Enhanced Raman scattering. *ACS Sens.* **9**, 4811–4821 (2024).
9. Traynor, S. M. et al. Review—Recent advances in electrochemical detection of prostate specific antigen (PSA) in Clinically-Relevant samples. *J. Electrochem. Soc.* **167**, 037551 (2020).
10. Krizkova, S. et al. Electrophoretic fingerprint Metallothionein analysis as a potential prostate cancer biomarker. *Electrophoresis* **32**, 1952–1961 (2011).
11. Liu, R. et al. Universal MOF nanozyme-induced catalytic amplification strategy for label-free electrochemical immunoassay. *Chin. Chem. Lett.* **35**, 109664 (2024).
12. Pandiyaraj, K., Elkaffas, R. A., Mohideen, M. I. H. & Eissa, S. Graphene oxide/Cu–MOF-based electrochemical immunosensor for the simultaneous detection of Mycoplasma pneumoniae and Legionella Pneumophila antigens in water. *Sci. Rep.* **14**, 17172 (2024).

13. Miao, M. et al. A simple electrochemical immunosensor based on MWCNTs-COOH/Fc-COOH@CoAl-LDH, nanocomposite for sensitive detection of the tumor marker CA724. *Int. Immunopharmacol.* **143**, 113406 (2024).
14. Zhang, Y., Zheng, Z. N., Lin, X. H., Liu, A. L. & Lei, Y. A homogeneous electrochemiluminescence immunoassay platform based on carbon quantum Dots and magnetic beads enrichment for detection of thyroglobulin in serum. *Talanta* **276**, 126205 (2024).
15. Du, Y., Jiang, S., Yuan, H., Cui, L. & Zhang, C. Facile fabrication of silica nanoparticles with incorporation of AIEgen and coreactant as self-enhanced electrochemiluminescence probes for sensitive immunoassay of microcystin-LR. *Sens. Actuators B.* **401**, 134906 (2024).
16. Hu, W. et al. Development of a Dual-Epitope Nanobody-Based immunosensor with MXenes@CNTs@AuNPs for ultrasensitive detection of rotavirus. *Anal. Chem.* **96**, 19678–19686 (2024).
17. Li, S. et al. Rapid detection of Salmonella in milk by labeling-free electrochemical immunosensor based on an $Fe_3O4$–ionic liquid-modified electrode. *Talanta* **270**, 125576 (2024).
18. Wang, Q., Xin, H. & Wang, Z. Label-free immunosensor based on polyaniline-loaded MXene and gold-decorated β-cyclodextrin for efficient detection of carcinoembryonic antigen. *Biosensors* **12**, 657 (2022).
19. Parajuli, D. MXenes-polymer nanocomposites for biomedical applications: fundamentals and future perspectives. *Front. Chem.* **12**, 1400375 (2024).
20. Li, K., Zhang, S., Li, Y., Fan, J. & Lv, K. MXenes as noble-metal-alternative co-catalysts in photocatalysis. *Chin. J. Catal.* **42**, 3–14 (2021).
21. Dmytriv, T. R. & Lushchak, V. I. Potential biosafety of mxenes: Stability, Biodegradability, toxicity and biocompatibility. *Chem. Record.* **24**, e202300338 (2024).
22. Cao, F. et al. Recent advances in oxidation stable chemistry of 2D MXenes. *Adv. Mater.* **34**, 2107554 (2022).
23. Lipton, J. et al. Mechanically strong and electrically conductive multilayer MXene nanocomposites. *Nanoscale* **11**, 20295–20300 (2019).
24. Cheng, Y., Jiang, B., Chaemchuen, S., Verpoort, F. & Kou, Z. Advances and challenges in designing MXene quantum Dots for sensors. *Carbon Neutralization*. **2**, 213–234 (2023).
25. Wan, M. et al. MXene quantum Dots enhanced 3D-printed electrochemical sensor for the highly sensitive detection of dopamine. *Microchem. J.* **184**, 108180 (2023).
26. Liang, H. et al. Dual-signal electrochemical biosensor for neutrophil gelatinase-associated Lipocalin based on MXene-polyaniline and Cu-MOF/single-walled carbon Nanohorn nanostructures. *ACS Appl. Nano Mater.* **5**, 16774–16783 (2022).
27. Hou, Y. et al. *Electrochemical Fiber Electrode Fabrication by Spinning: State-of-the-Art and Perspectives* (ACS Electrochemistry, 2025).
28. Liu, K. et al. Flexible electrode materials for emerging electronics: Materials, fabrication and applications. *J. Mater. Chem. A*. **12**, 20606–20637 (2024).
29. Li, Y. et al. Boosting the photocatalytic ability of g-C3N4 for hydrogen production by $Ti_3C_2$ MXene quantum Dots. *ACS Appl. Mater. Interfaces*. **11**, 41440–41447 (2019).
30. Yan, H. et al. Ti3C2 MXene quantum Dots decorated mesoporous $TiO_2$/$Nb_2O_5$ functional photoanode for dye-sensitized solar cells. *Opt. Mater.* **140**, 113902 (2023).
31. Safarpoor, M. et al. Podophyllotoxin extraction from Linum usitatissimum plant and its anticancer activity against HT-29, A-549 and MDA-MB-231 cell lines with and without the presence of gold nanoparticles. *Appl. Organomet. Chem.* **32**, e4024 (2018).
32. Ren, E. et al. Facile synthesis of $V_2CTx$@RGO composite aerogel via hydrothermal reaction and its dye adsorption performance. *J. Mater. Sci.: Mater. Electron.* **34**, 343 (2023).
33. Yang, J. et al. MXene-AuNP-Based electrochemical aptasensor for Ultra-Sensitive detection of Chloramphenicol in honey. *Molecules* **27**, 1871 (2022).
34. Singh, R., Kumar, S., Bera, S. & Bhunia, S. K. Trends in using fluorescent MXene quantum Dots for selective detection and bioimaging applications: a review. *ACS Appl. Nano Mater.* **6**, 19526–19550 (2023).
35. Yang, E. J. et al. Room temperature manufacturing photoluminescent graphene quantum Dots based on MXene. *Carbon* **167**, 863–869 (2020).
36. Xue, Q. et al. Photoluminescent $Ti_3C_2$ MXene quantum Dots for multicolor cellular imaging. *Adv. Mater. (Deerfield Beach Fla)*, 29 (2017).
37. Ai, F. et al. Amino-Functionalized Ti3C2 MXene quantum Dots as photoluminescent sensors for diagnosing histidine in human serum. *ACS Appl. Nano Mater.* **4**, 8192–8199 (2021).
38. Cai, G., Yu, Z., Tong, P. & Tang, D. $Ti_3C_2$ MXene quantum dot-encapsulated liposomes for photothermal immunoassays using a portable near-infrared imaging camera on a smartphone. *Nanoscale* **11**, 15659–15667 (2019).
39. Ranjbari, S., Hatamluyi, B., Aghaee-Bakhtiari, S. H., Rezayi, M. & Arefinia, R. A label-free electrochemical biosensor based on PBA-Au-MXene QD for miR-122 detection in serum samples. *Microchim. Acta*. **190**, 482 (2023).
40. Safaei, M. & Shishehbore, M. R. Energy conversion and optical applications of MXene quantum Dots. *J. Mater. Sci.*, 1–37. (2021).
41. Liu, Y., Zhang, W. & Zheng, W. Quantum Dots compete at the acme of MXene family for the optimal catalysis. *Nano-Micro Lett.* **14**, 158 (2022).
42. Azam, M. A. et al. X-ray diffraction and photoelectron spectroscopy analyses of MXene electrode material used in energy storage applications–a review. *Mater. Test.* **66**, 760–785 (2024).
43. Traynor, S. M. et al. Soleymani, recent advances in electrochemical detection of prostate specific antigen (PSA) in clinically-relevant samples. *J. Electrochem. Soc.* **167**, 037551 (2020).
44. Xu, H., Zheng, D., Liu, F., Li, W. & Lin, J. Synthesis of an MXene/polyaniline composite with excellent electrochemical properties. *J. Mater. Chem. A*. **8**, 5853–5858 (2020).
45. Ahmad, M., Shuja, A., Murtaza, I., Fahad, S. & Khan, M. S. Synergistic integration of MXenes with conducting polymers to enhance the specific capacitance of asymmetric supercapacitors. *J. Mater. Sci.: Mater. Electron.* **36**, 1096 (2025).
46. Zhang, A., Wang, Y., Yu, H. & Zhang, Y. Three-Dimensional printed MXene@ PANI hierarchical architecture for High-Performance Micro-Supercapacitors. *Materials* **18**, 2277 (2025).
47. Magar, H. S., Hassan, R. Y. & Mulchandani, A. Electrochemical impedance spectroscopy (EIS): Principles, construction, and biosensing applications. *Sensors* **21**, 6578 (2021).
48. Robinson, C., Juska, V. B. & O'Riordan, A. Electrochemical Impedance Spectroscopy (EIS) Based Label-Free Immunosensors, (2022).
49. Rathaur, V. S., Gokhale, N. A. & Panda, S. pH effects on capture efficiency and deposition patterns in sessile droplet immunoassays: An XDLVO analysis, Biomicrofluidics, 18 (2024).
50. Cao, L. et al. Uncovering the interplay between pH receptors and immune cells: potential drug targets. *Oncol. Rep.* **46**, 1–14 (2021).
51. Zhang, M. et al. PSA detection electrochemical immunosensor based on MOF-235 nanomaterial adsorption aggregation signal amplification strategy. *Microchem. J.* **171**, 106870 (2021).
52. Hua, X., Zhao, T., Gui, X. & Jin, B. A NiFe PBA/AuNPs nanocomposite sensitive immunosensor for electrochemical detection of PSA. *Anal. Methods*. **16**, 1923–1933 (2024).
53. Yue, Y. et al. Ultrasensitive detection of PSA in human serum using Label-Free electrochemical biosensor with magnetically induced Self-Assembly based on α-$Fe_2O_3$/$Fe_3O_4$@Au nanocomposites. *Microchem. J.* **201**, 110487 (2024).
54. Li, S. et al. Electrochemical immunosensor based on hybrid $MoS_2$/Pt@Au-nanoprism/PDA for simultaneous detection of free and total prostate specific antigen in serum. *Sens. Actuators B.* **357**, 131413 (2022).

55. Yan, L., Xu, S. & Xi, F. Disposal Immunosensor for Sensitive Electrochemical Detection of Prostate-Specific Antigen Based on Amino-Rich Nanochannels Array-Modified Patterned Indium Tin Oxide Electrode, *Nanomaterials*, **12** 3810. (2022).
56. Zhang, H., Qu, H., Cui, J. & Duan, L. A simple electrochemical immunosensor based on a chitosan/reduced graphene oxide nanocomposite for sensitive detection of biomarkers of malignant melanoma. *RSC Adv.* **12**, 25844–25851 (2022).
57. Moon, J. M., Hui Kim, Y. & Cho, Y. A nanowire-based label-free immunosensor: direct incorporation of a PSA antibody in electropolymerized polypyrrole. *Biosens. Bioelectron.* **57**, 157–161 (2014).
58. Yang, M., Javadi, A. & Gong, S. Sensitive electrochemical immunosensor for the detection of cancer biomarker using quantum Dot functionalized graphene sheets as labels. *Sens. Actuators B.* **155**, 357–360 (2011).
59. Darvishi, E., Ehzari, H., Shahlaei, M., Behbood, L. & Arkan, E. The electrochemical immunosensor for detection of prostatic specific antigen using quince seed mucilage-GNPs-SNPs as a green composite. *Bioelectrochemistry* **139**, 107744 (2021).

## Acknowledgements

AcknowledgementsThe authors gratefully acknowledge the Nanotechnology Research Center of Tehran University of Medical Sciences (Approval No. IR.TUMS.TIPS.REC.1402.134) for their financial support.

## Author contributions

M. S.: Methodology, Investigation, Software; Formal analysis; Writing - Original Draft, Writing - review & editing A. A.: Methodology, Validation, Formal analysis, Investigation, Writing - original draft, Writing - review & editing. M. G.: Supervision, Methodology; Writing - review & editing, Methodology; Validation, Investigation., R. D.: Supervision, Conceptualization, Methodology; Writing - original draft, Writing - review & editing, Validation, Project administration; Resources; Funding acquisition.,

## Funding

The project was funded by the Nanotechnology Research Center of Tehran University of Medical Sciences, Iran (Approval No. IR.TUMS.TIPS.REC.1402.134).

## Declarations

## Competing interests

The authors declare no competing interests.

## Additional information

**Supplementary Information** The online version contains supplementary material available at https://doi.org/10.1038/s41598-025-26754-y.

**Correspondence** and requests for materials should be addressed to M.G. or R.D.